III Experimental Setup

In this chapter the electron accelerator facility, the target and the detectors are discussed. The choice of the kinematic configurations is motivated.

3.1 The electron beam

For the measurements described in this thesis, the electron beam provided by the Amsterdam Pulse Stretcher facility (AmPS) was used. This facility consists of a linear electron accelerator with a low duty-factor and a storage-stretcher ring. When operated in storage mode, experiments with gaseous targets internal to the ring are performed in the IT hall. In stretcher mode – the mode used for the present experiment – the injected bursts of electrons are extracted as an almost continuous current for experiments in the EMIN hall. A view plan of the facility is shown in Fig. 3.1.

The Medium Energy Accelerator (MEA) [Vri84] provides a beam of electrons in short bursts up to 2.1 μs with a repetition rate of at maximum 150 Hz. The energy can be varied continuously up to 700 MeV at zero current. An energy spectrum compression system brings the energy spread down to less than 0.1%. The electrons are subsequently injected into a stretcher ring (the AmPS proper) with a circumference of 212 m [Wit93]. This length corresponds to a revolution time of 708 ns. A closed orbit for the recirculating electrons is defined by a lattice of 32 dipoles, 68 quadrupoles, and 32 sextupoles.

As the electrons are bent in the arcs of the ring, they loose energy due to synchrotron radiation, which is compensated by an additional RF cavity inside the ring. To obtain extraction from the ring, the RF voltage inside this cavity is gradually reduced. This causes shrinking of the phase space area for stable circulation [Wu91]. In the unstable phase space region, electrons suffer large excursions from the beam centre. At a distance of about 25 mm from the beam centre line, an electrostatic septum intercepts the particles and enlarges their separation with respect to the stable recirculating beam using an electric
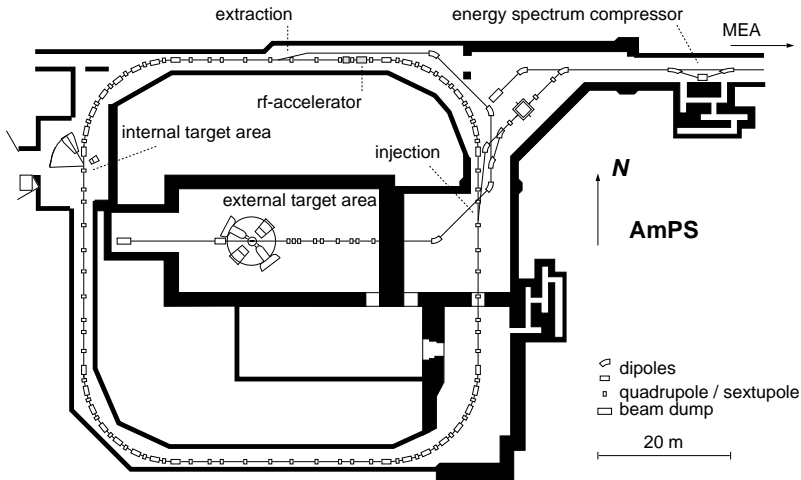
Figure 3.1: *Floor plan of the AmPS facility. Of the MEA linear accelerator only the energy spectrum compressing system is shown. The experiment was performed in the external target area EMIN.*

field [Lin92]. The extracted beam is then guided to the target area by magnetic elements.

The extraction time can be varied to a maximum of 20 ms, limiting the MEA repetition rate to values above 50 Hz for a continuous beam. The optical configuration of the ring allows for at most three-turn injection.

Experimental conditions

For all kinematic settings of this experiment MEA was operated at a repetition rate of 50 Hz and a burst length of 2.1 μs. The electrons injected into the AmPS ring were extracted over a period of 20 ms with a *macroscopic* duty factor of more than 80%. This duty factor varied by no more than 10% during the experiment. In order to obtain the highest macroscopic duty factor, the lowest possible repetition rate compatible with the required luminosity was selected.

Inhomogeneities in the beam structure at the sub-microsecond time scale give rise to a time-difference distribution of the accidental coincidences which is not flat [Ond98b]. It is therefore advantageous to optimize this *microscopic* duty factor, which is mainly sensitive to details of the injection process.
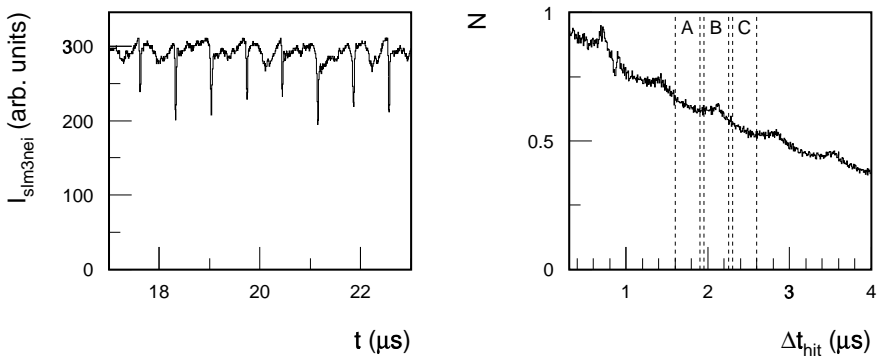
Figure 3.2: *The beam structure at time scales close to the revolution time in-fluences the instantaneous luminosity at the target and the effective real-to-accidental ratio. The left panel shows the instantaneous current in the AmPS ring as a function of time. The right panel shows the time difference distribution between two successive hits in a ho-doscope strip of the HADRON3 detector.*

The severity of these inhomogeneities can be estimated by investigating the time difference distribution of successive events in a fast-counting detector. Changes in the instantaneous current that are due to the revolution time in the ring will give rise to a peaked structure with a periodicity of 708 ns (see Fig. 3.2, right panel). Following [Sta99b], an intensity asymmetry

$$A = \frac{N_B - \frac{1}{2}(N_A + N_C)}{N_B + \frac{1}{2}(N_A + N_C)} \tag{3.1}$$

can be defined, where N_i is the number of events in the time interval i as shown in the right panel of Fig. 3.2. All intervals are 300 ns wide. This intensity asymmetry is a measure for the relative surplus of counts in region B, which is centred around Δt=2100 ns, with respect to the expected yield in this area as derived from the average in A and C. For the distribution shown in Fig. 3.2, the intensity asymmetry is 2.2%.

To ensure a continuous current at the 708 ns time scale, three-turn injection was used during the entire experiment. In this mode, injection of electrons from MEA continues while electrons already circulating in the ring pass the injection point undisturbed. The optical properties of the ring and the pulse

length of 2.1 μs allow for three-turn injection. A mismatch between burst length
and revolution time will now cause a reduction to only 2/3 of the maximum
circulating current. The effect on the time-structure of the beam will then be
only minor. The intensity asymmetry A was monitored continuously during the
experiment. It was always less than 5%.

For this experiment, the incident electrons had an energy of 563.7±0.3 MeV
as determined with elastic scattering measurements from ^{12}C and ^{3}He, per-
formed several times in between the coincidence measurements (see section 4.5).

3.2 Target setup

The target setup consisted of a cryogenic, high-pressure 'barrel' cell contain-
ing gaseous ^{3}He, a graphite target with a thickness of 93.5 mg/cm^2 and an
aluminium-oxide target for beam calibration purposes.

The barrel cell is a cylindrically shaped container with a diameter of 50 mm
and an aluminium wall with a thickness of 250 μm [Una91]. At the top-side of
the container a heat-exchanger is mounted consisting of 34 copper ribs. This heat
exchanger is connected to a cold head. A cryogenic refrigerator with a capacity
of 30 W at 18.5 K is used. Between the ^{3}He gas and the heat exchanger, heat is
transported by natural convection.

Temperature sensors are mounted directly on top of the heat exchanger. The
cell can hold a pressure of 4 MPa at temperatures around 20 K. A 5 MPa pressure
sensor is mounted outside the scattering chamber in the filling line of the target.
The cell can be moved vertically by a pneumatic system connected to the cold
head in such a way that the solid targets can be positioned at beam height
by means of a stepping motor. Both target selection systems are controlled
remotely.

The cell is connected to a closed-circuit gas-handling system containing a
supply of ^{3}He at 3 MPa, a compressor and a 5 l emergency recuperation ves-
sel. A PLC system monitors the pressure sensor and will open a valve to the
recuperation vessel if the cell pressure exceeds specified safety limits. The setup
is designed such that cooling failures will not result in loss of ^{3}He gas. The
system avails of a cold-trap which can be used to remove contamination from
the recuperated ^{3}He which might freeze in the filling lines to the target.

The recuperation vessel can also be used to temporarily store the ^{3}He gas whilst performing measurements with a different gas (*e.g.*, Hydrogen) or background measurements with an empty cell.

During the experiment the recuperation system was used several times and no loss of ^{3}He gas was observed. All measurements with the ^{3}He gas-target were performed at a temperature of 15 K and a pressure of 2.9 MPa, as determined by the sensors attached. The effective target thickness was determined by elastic scattering measurements as described in section 4.5.

The carbon target

In order to perform measurements of the absolute detection efficiency of the electron detector system, a graphite target of 93.5 mg/cm^2 was used. This fixed target can replace the barrel cell at beam height and be rotated remotely. Angles from 50 to 120 degrees with respect to the incident beam can be reached. The homogeneity of the target is better than 1%.

3.3 Detection of the scattered electron

The scattered electrons were detected in the QDQ magnetic spectrometer. This focussing spectrometer can detect electrons within a range of $\pm 4.5\%$ with respect to the selected central momentum value. The momentum resolution is better than 2×10^{-4} [Vri90]. The solid angle is defined by an octangular slit with an acceptance of ± 70 mrad in both the in-plane and out-of-plane direction. The detector package consists of two pairs of multi-wire drift chambers (MWDCs) [Dis84], a thin (3 mm) 'bottom'-scintillator covering the same area as the wire chambers, twelve 'timing'-scintillator paddles (8 mm) segmented in the dispersive direction, an aerogel Čerenkov detector and a 'top'-scintillator (4 mm). The index of refraction of the aerogel material is n=1.05. The bottom- and top-scintillators are read out on both sides by a photomultiplier tube. A cross section of the detection package is shown in Fig. 3.3.

The trigger for electrons is defined as a coincidence between a hit in the bottom-scintillator and any of the twelve timing-scintillators. The phase of the trigger is determined by the timing-scintillators. Information from the aerogel Čerenkov detector is only used in the off-line analysis.
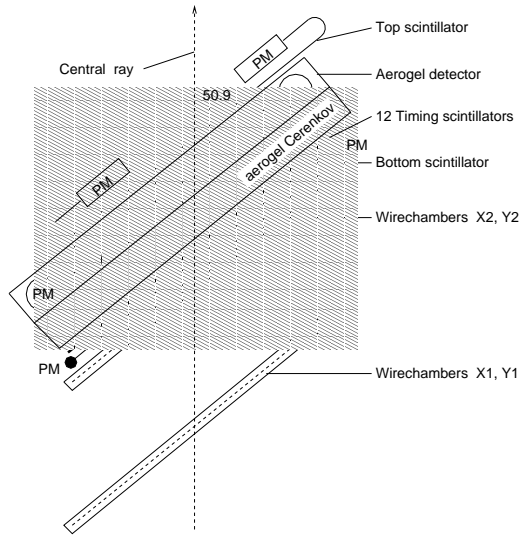
Figure 3.3: *The focal plane detection package of the QDQ magnetic spectrometer.*

The position information in the successive wire chambers is used to reconstruct the momentum vector at the target [Vri90]. Information is also obtained on the vertex position (y_{tg}) perpendicular to the optical axis of the spectrometer with a resolution of 1 mm. The solid angle covered by the spectrometer has been found to be dependent on the vertex position for $y_{tg} < -6.0$ mm or $y_{tg} > 3.0$ mm [Spa97].

3.4   Proton detectors

To detect the protons emitted from the target two scintillator detectors were used: HADRON3 and HADRON4. These detectors both cover a large solid angle and span a sizeable range in detected proton energies [Mul95, Pel96, Pel99]. The design of both HADRON detectors is similar and the differences will be noted only where relevant.

As these detectors are non-magnetic, the scintillation material is directly exposed to all particles emitted from the target. At the anticipated luminosity (above 10^{35} atoms/cm^2 s) this requires a setup with a large granularity to be
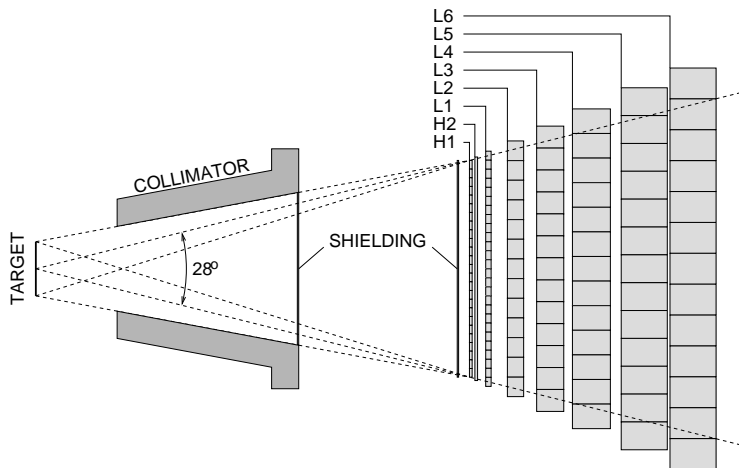
Figure 3.4: *A top view of the HADRON3 detector. The detector housing is not shown. The distance between the target and the front of the first hodoscope layer H1 is 800 mm.*

able to cope with the count rate in each individual element. A top view of the HADRON3 detector is shown in Fig. 3.4. Its design is guided by the results of extensive beam tests with scintillators and absorbers of various dimensions [Zon94].

The detection system proper consists of a pair of thin, perpendicularly segmented 'hodoscope' strips to determine the impact position, and a series of larger 'stopping' layers to measure the proton energy and perform particle identification. In front of the hodoscope shielding material may be mounted to reduce the flux of low-energy particles. At the same time this shielding will raise the detection thresholds for protons. The active detection elements consist of BC408 plastic scintillator material and are mounted inside a light-tight lead housing with a thickness of 50 mm on the front side and 30 mm at the sides and at the back. In this experiment HADRON3 was operated with 5.2 mm lead shielding, giving an effective lower detection threshold for protons of 72 MeV. HADRON4 was operated with stainless steel shielding of 2.0 mm (lower threshold 48 MeV) or 1.0 mm (36 MeV).

In between the housing and the scattering chamber a lead collimator with a wall thickness of 50 mm is installed to prevent the influx of particles not

originating from the target. An extended target of ± 100 mm is allowed for. The distance between the target and the first hodoscope plane (H1) is 800 mm.

For each scintillator element the generated light is collected in a photomultiplier tube (PM). For the thin (2 mm) hodoscope elements of HADRON4 PMs are attached to both ends of the scintillator to counter losses due to the strong attenuation in these 640 mm long strips. The high-voltage applied to each PM can be individually adjusted to match the input sensitivity of the charge digitizers.

The hodoscopes and the first stopping layer (L1) require a high degree of segmentation to cope with the high flux of low-energy electrons coming from the target. Besides, this segmentation is needed to obtain an accurate determination of the impact position of the impinging particles. The effective width of the in-plane-segmented hodoscope H1 and of L1 is identical, but offset by half the width of one element to increase the in-plane angular resolution. In the subsequent stopping layers, the segmentation is reduced. The increasing width of the elements in the back layers takes the additional angular spread due to multiple scattering and hadronic interactions into account.

Characteristic parameters for both HADRON detectors are given in Table 3.1.

Data acquisition

Given the high count rate per element (up to 1 MHz) and the need for complex trigger decisions, the analogue signals from the PMs are digitized per element immediately on arrival. In this way the dead time of the DACQ is minimized to the combined effect of channel and detector-trigger dead time. In this way, time needed for global trigger decisions and for readout of the data from the channels does not introduce additional dead time.

The digitizers ('frontends') are constructed as triple-height VME modules, with the standard VME bus supplemented with trigger and DACQ control lines. Each VME board contains two independent frontends. As the digitizers are autonomous units, they use an internal logic condition as the start-of-measurement: integration of the analogue signal starts when both the slope ('low' threshold) and the height ('high' threshold) exceed the specified discriminator levels. At the same time the time-to-amplitude converter (TAC) is started, the phase of which is determined by the differential, 'low' discriminator to minimize rise-time effects in the time integration process. Both charge and arrival time (relative to

Table 3.1: *Characteristic parameters of both HADRON detectors. Nominal values are shown; the actual values during the experiment or used in the analysis of the measurements may depend on the shielding installed and the cuts applied to the data during the analysis.*

	HADRON3	HADRON4
number of scintillators	141	94
number of photomultipliers	141	134
hodoscope segmentation	25	20
hodoscope width per element (mm)	16	32
L1 elements (subtriggers)	26	21
opening angle, in-plane and out-of-plane (deg)	28	44
in-plane angular resolution (deg)	0.5	1
out-of-plane angular resolution (deg)	1	2
subtended solid angle (msr)	230	540
number of stopping layers	6	4
$T_p^{\min}$ (MeV)	36	25
$T_p^{\max}$ (MeV)	239	165

the detector trigger) are determined. Besides, every frontend avails of a direct ('hit') logic output which may be used as input to the detector trigger modules. All relevant parameters (offset and width of the charge and time integration, signal thresholds and the 'hit' delay) can be set by VME commands [Zon94].

If a valid detector trigger is generated, a time-stop signal is provided to the frontends using the special-purpose part of the crate backplane. This signal stops the TACs and starts the digitization of the charge integrator and TAC voltages. The converted values are subsequently stored in a 64-word deep cyclic buffer in dual-port memory (DPM). The frontend electronics is reset if no time-stop signal arrives within a certain time after the TAC has reached its maximum value.

Because at most 19 digitizer modules can be mounted in one crate, the frontend electronics spans four VME-crates per detector. Every crate contains a data-acquisition and readout transputer (DART) [Kwa91] which manages the special-purpose bus-lines and controls the VME bus for data readout. Amongst other functions, the DART determines the address of the digitized information

in the DPM cyclic buffer of each frontend, using the special-purpose part of the crate back plane. When requested, the information is retrieved by the DART and stored as sub-event in its local event fragment memory (EFM). These sub-event fragments are combined by the acquisition transputer chain into complete HADRON events to be provided to the event builder (EB).

Trigger

To limit the trigger rate to an acceptable level of at most 800 kHz, signals from various elements are combined. Taking advantage of the segmented design, coincidences of hits in elements in subsequent layers are taken as trigger condition. To keep the detection threshold for protons as low as possible, the first two layers with identical orientation are used, *i.e.*, H1 and L1. As the elements in these layers are offset with respect to each other, a coincidence between the L1 'hit' signal and the logic OR of both corresponding H1 strips is used to generate the subtrigger (T1A). The OR of these subtriggers is then made (T1B) and used as detector arm trigger (ATR). For HADRON4 the OR of the 'hit' signals from both sides of an H1 element is used in T1A.

The phase of the final subtrigger is determined by the arrival of the 'hit' signal from the L1 elements. The width of the acceptance window – started by any of the corresponding H1 hits – is computer controllable. Care is taken to ensure that the signals from real tracks are well within the acceptance of the gate.

Tools for efficiency determination

The HADRON detector has two sources of dead time: the process of digitization in each frontend and the dead time associated with the processing of the trigger.

The frontend dead time is due to the local digitization process and its duration is around 110 ns, depending on the adjustable parameters of the TAC. To monitor the induced inefficiency, an electronic test pulse is sent at regular intervals to all digitizer modules. A dedicated digitizer module is employed to determine the total number of test pulses generated. The live time per frontend is determined using the acceptance ratio deduced from these test pulses.

The same quantity is also measured by flashing a preset amount of light either into the scintillation material or directly into the PM. A photo diode is employed to detect these laser-generated flashes and its signal is digitized in the same way as the regular events. The live time determined with the laser flasher has been found to be identical to the one determined with the test pulse [Pel96].

In this experiment the determination of the frontend live time is based solely on test pulse data. It is lowest in the two hodoscope layers, as they suffer from a high flux of low-energy particles, but was always higher than 80%. The L1 live time was above 99% because of the high threshold set for these triggering elements. The live time of the other stopping layers was better than 93% and 90% for HADRON3 and HADRON4, respectively.

The dead time due to the trigger is set at a fixed value of 250 ns. To determine the trigger live time, a prompt output with negligible dead time is provided by the trigger module. The ratio of generated arm triggers (who are subject to the 250 ns dead time) over the number of prompt triggers determines the trigger live time and is applied as a correction factor to the data.

The trigger live time during this experiment was always better than 77%.

3.5   Coincidence detection

In an $(e, e'pp)$ reaction, the two protons will be emitted from the vertex at the moment the nucleus is struck by the electron. In this case, all three detectors (QDQ, HADRON3 and HADRON4) will give an arm trigger (ATR) within an interval of several hundred nanoseconds. However, such a coincidence can also be due to particles that originate from different nuclear reactions, that occur accidentally at roughly the same time. To estimate the fraction of the accidental events that contribute to the three-fold coincidence time region, a coincidence detector (CD) is employed, that measures the arrival times of the three ATR signals with a resolution of 48.8 ps [Ver96]. Each ATR starts a 'window' with a set length of 125 ns. These window signals are used by the gating and prescaling module to classify events based on their coincidence type (single, double or triple). The readout of each type of coincidence event can be individually enabled and prescaled using a special module in the CD. The readout of the various types of events is completely independent as long as the total event rate does

not exceed 5 kHz or 1.4 MByte/s. In this experiment all three-fold coincident events (triples) were stored as well as a subset of the doubles and singles for monitoring purposes.

So as not to load unnecessarily the data links with the transport of unneeded event fragments (from arm events which did not take part in one of the selected coincidences) an event fragment labelling system is used. Together with the ATR signal from the detector arm, an ATR label is sent to the CD. If the event-fragment is deemed 'interesting', this label, together with an event trigger (ETR), is sent back to the detector arm. The event-fragment data is then collected from the sub-event builders in the various crates and transported, together with the arrival time information from the CD, to the event builder (EB). Using this labelling system events can be retrieved asynchronously. Counters internal to the event data are used to check the consistency of the combined events. Besides, triple events due to test pulses delivered simultaneously to both HADRON detectors and the QDQ are used to perform off-line consistency checks.

3.6   Kinematic conditions

In order to enhance the contribution due to knockout of correlated proton pairs to the cross section, measurements are preferably performed in the so-called 'dip' region. Here, sufficient energy is transferred to the nucleus to emit two high-energy nucleons (above the detection threshold of the HADRON detectors), while at higher energy transfers the contribution from Δ excitation is expected to increase.

Several constraints determine the accessible kinematic configurations:

- the beam energy is restricted to less than 600 MeV. Higher energies limit the available beam current and make the accelerator more sensitive to failure.

- the central detection angle of the scattered electron should be larger than $27°$ due to geometrical limitations which prevent the QDQ spectrometer to move closer towards the beam pipe.

- the transferred energy should be sufficient for both protons to deposit a reasonable amount of energy in both HADRON detectors, taking into

account the detection thresholds of HADRON3 and HADRON4, namely 72 MeV and 48 MeV, respectively. (with reduced shielding the threshold for HADRON4 becomes 36 MeV)

- preferably, all measurements should be performed at the same incident energy to reduce the overhead due to accelerator and ring tuning.

Kinematic configurations were selected in accordance with the aforementioned limitations. To investigate the coupling mechanism of the virtual photon to the ^{3}He system, measurements were performed at various values of the three-momentum transfer q. A series of measurements at various energy transfer values allowed study of the reaction mechanism as a function of the invariant energy of the photon and two-proton final state. In this way, the relative importance of one-body and two-body hadronic currents can be investigated.

At beam energies below 600 MeV and small electron scattering angles (27°), the dip region corresponds to energy transfer values around 200 MeV. The wish to measure at missing-momentum values around 0 MeV/c requires that ω be at least around 220 MeV.

At $\omega = 220$ MeV the requirement that $\theta_{e'} > 27°$ gives a minimum momentum transfer q of 305 MeV/c at an incident energy $E_0 = 564$ MeV. Higher incident energies raise this q-value, lower E_0 reduces the flux of virtual photons. The setting is symbolically labelled LQ in the remainder of this thesis.

Besides, extensive investigations have been made to find kinematic configurations where the influence of final-state interactions might be minimized. This search was guided by the continuum Faddeev calculations [Gol95] as described in section 2.3. Within the accessible kinematic domain, LQ is the only kinematic setting that contains two-proton angular combinations where the calculated full cross section, calculated with a one-body hadronic current, is identical to the plane-wave prediction. These have been measured in the kinematic setting labelled PEF.

The ω value of 220 MeV was chosen to perform measurements at various momentum transfer values. Three values of transferred momentum were selected: 305 (LQ), 375 (CQW) and 445 (HQ) MeV/c, where the choice of q=445 MeV/c was dictated by the strongly reduced count rate at higher values of q. The esti-
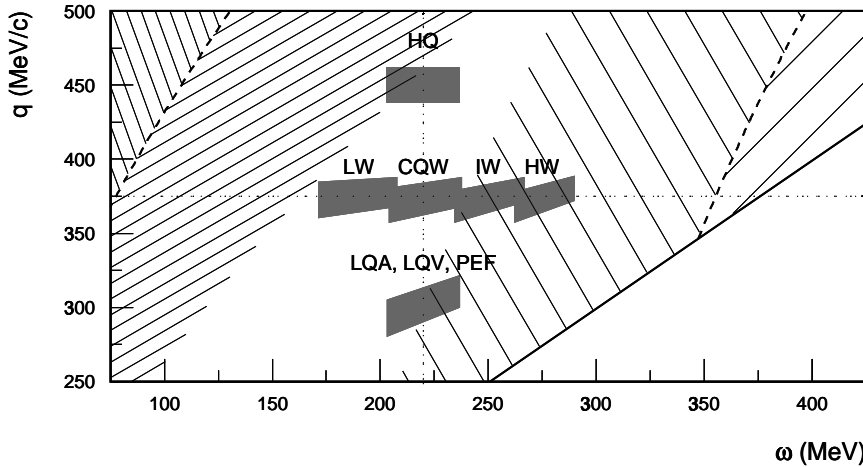
Figure 3.5: *Shaded areas indicate the coverage in (ω, q) due to the acceptance of the QDQ spectrometer. The dashed lines indicate kinematic conditions corresponding to quasi-elastic knockout (left-hand side) or excitation of the Δ resonance (right-hand side). Hatched regions indicate the width (FWHM) as calculated by the code QFS, due to [LiO88]. Symbolic names of the kinematic settings are indicated.*

mated count rate for HQ is 20 times smaller compared to estimates for the LQ setting.

At q=375 MeV/c, measurements at several energy transfer values were performed in such a way that a continuous range from 170 MeV to 290 MeV was covered with small overlaps between the different settings. Within this range, the invariant mass of the two-proton system in the final state, $W_{p_1' p_2'}$, ranges from 2005 to 2120 MeV/c^2. At the low-ω point (LW) the shielding of the backward proton detector HADRON4 was reduced to gain detection volume in the region of low missing momenta. This required a 50% reduced luminosity with respect to other kinematic settings at the same proton detection angle.

The coverage of transferred momentum and energy – determined by the acceptance of the QDQ spectrometer – is indicated in Fig. 3.5.

The positioning of the two proton detectors was guided by the emission of the protons at conjugate angles. The angle of the forward proton detector, HADRON3, was determined by geometrical constraints of detector housing and beam pipe. The angle between q and the forward proton was kept as small as possible. The backward proton detector was located around the conjugate angle, corresponding to the kinematic configuration where the neutron is left at rest in the final state.

The LQ kinematic setting, which features the largest flux of virtual photons, was used to perform additional measurements at other proton angles to investigate the angular correlation and the behaviour of the cross section as a function of the angle γ_1 between q and the forward proton.

An overview of all measured kinematic settings is given in Table 3.2.

Table 3.2: *Overview of the kinematic configurations of the ^{3}He$(e, e'pp)$ experiment. The incident energy was 563.7 MeV. The transferred four-momentum $Q^2 = q^2 - \omega^2$ is indicated.*

ID	ω (MeV)	q (MeV/c)	$\theta_{e'}$ (deg)	θ_q (deg)	Q^2 (GeV/c)^2	θ_{H3} (deg)	θ_{H4} (deg)
LQA	220	305	-27.72	31.6	0.045	53.8	-120.4
LQV						53.8	-92.9
PEF						79.9	-100.1
CQW	220	375	-40.26	36.4	0.092	53.8	-105.3
HQ	220	445	-52.01	37.6	0.150	53.8	-119.7
LW	190	375	-41.14	41.0	0.110	53.8	-119.7
IW	250	375	-38.72	31.6	0.078	53.8	-105.3
HW	275	375	-36.76	27.5	0.065	53.8	-105.3